Fibrillar Structure of Nafion: Matching Fourier and Real Space Studies of Corresponding Films and Solutions

L. Rubatat, G. Gebel, and O. Diat*

Département de Recherche Fondamentale sur la Matière Condensée, SI3M, Groupe Polymères Conducteurs Ioniques, CEA Grenoble, 17 rue des Martyrs, 38054, Grenoble Cedex 9, France

Received February 16, 2004; Revised Manuscript Received July 6, 2004

ABSTRACT: Using both scattering and microscopy techniques, we have characterized the complex Nafion structure over a large range of length scales. Analysis of experimental data from dry membrane to aqueous dispersion suggests an intrinsic fibrillar structure. The fibrils correspond to elongated polymeric aggregates surrounded with the ionic charges. In the Nafion membrane, the fibrils are entangled and collapsed with a degree of orientation at the mesoscopic scale. Upon swelling and temperature treatment, these aggregates are hydrated and dispersed in a colloidal suspension.

Introduction

In earlier papers, we have introduced evidence that cylindrical aggregate is an important motif in Nafion solution[1,2] and in highly swollen membranes.[3] In this article, we extend this study to hydrated membranes with lower water content. Using both microscopy and small angle scattering (SAS), we investigate the structure of these aggregates and their spatial packing in both solution and membrane states. One of the main reasons for this work on Nafion membranes (produced by du Pont de Nemours) and solutions is that they are benchmark systems for low temperature (<100 °C) fuel cells based on polymer electrolytes:[4,5,6] these perfluorosulfonic acid (PFSA) membranes[7,8,9] have excellent proton conductivity and chemical stability in stationary operation.[10] When a new proton exchange membrane is developed, its physicochemical and electrochemical properties are always compared with those of Nafion.[11,14,16] The corresponding solution state[11,12] is necessary for volumetric electrodes processing where catalytic and carbon particles are mixed together with the Nafion dispersion for optimizing electrode−membrane interfaces.[13] In these PFSA membranes, structure and ion transport properties are strongly correlated;[11,17,18] the proton conductivity of native or recast membranes is attributed to the existence of a nanostructure with a sharp interface between hydrophobic and hydrophilic domains. The theoretical models developed to quantify the relationships between water content and ion conductivity are mainly based on the solvation of spherical ionic nanoclusters, usually called inverted micelles in analogy with surfactant systems.[19−27] In an aqueous medium, depending on the ionic charge content, these clusters swell, percolate, and grow as a coalescence process.[28] However, numerous problems emerge in implementing this picture. For example, the percolation threshold in water volume fraction determined in conductivity is quite low (<10%) or the existence and the distribution of some crystalline zones are not so well explained. Experiments also show some anisotropic properties,[29−31] which has to be taken into account in the models. These aspects can be taken into account by considering an ionic and aqueous cylindrical network[32,33] embedded in the polymeric matrix or developing planar ionic geometries.[34−38] However, these approaches leave open problems. For example, how can we describe physically a strong reorganization of the polymer matrix[39] in order to explain either the continuous swelling from dry to Nafion dispersion or the corresponding development of transport properties between a native and a annealed cast membrane? Finally, ultralow angle scattering techniques reveal a more complex structural organization,[40,45] at least up to the micrometer scale, that is not yet understood and that previous models do not take into account. For these reasons, this study was carried out over a large water content variation. Taking into account simultaneously the observations at all the different scales and those from our previous results,[3] it seems logical to consider that the rodlike structure preexists in the dry Nafion membrane.

SAS is a very suitable technique to probe the topology of the hydrophilic/hydrophobic phase separation but only if it is applied over a range of scattering angles corresponding in the complete range of length scales exhibiting density modulation. However the lack of periodicity in these membrane systems prevents a simple analysis of the scattering data. Elliot et al.[46] have applied a powerful maximum-entropy method for the inversion of small-angle X-ray diffraction patterns. In this case, the electron density reconstruction depends on the wave vector range over which the fit procedure is applied. In Elliot's work, this was done over 1 decade and half of the **q**-vectors while we have shown that the scattered intensity varies over more than 3 decades. Consequently, parts of the long-range correlation from intra and/or inter scattered particles were missed. Another approach is to perform a 2D chord analysis as in ref 47. However, this procedure encounters the same problem: the characteristic correlation lengths extracted from this method do not allow to define unambiguously the morphology of the ionic and hydrophobic domains and their spatial distribution in an apparent isotropic polymeric system. To avoid most of these difficulties, we performed simultaneous studies in both real and Fourier spaces as a function of the water content, from a dry membrane to a colloidal suspension. Our objective is to obtain a coherent picture of the Nafion structure at different length scales and in both spaces. Our model is based on the existence of elongated

* Corresponding author: Telephone: 33 4 3878 9171. Fax: 33 4 3878 5691. E-mail: odiat@cea.fr.

10.1021/ma049683j CCC: $27.50
Published on Web 09/08/2004

polymeric aggregates surrounded by ionic groups and water molecules as was demonstrated in a previous paper.[3] In contrast to the Gierke model, the aqueous part of a hydrated Nafion membrane is considered as a swelling medium between these aggregates. This swelling will thus be analyzed as a dilution process allowing the disentanglement of the particles. As noted before, our study includes the Nafion solutions since this system received scanty attention,[48−52] compared to the membrane studies of direct relevance for applications;[53−56] Lopinnet et al.[2,57] have clearly shown, using scattering methods and analyzing the dispersion viscosity as a function of the solvent polarity and added salt, that a Nafion solution may be considered as a polyelectrolyte system formed by rodlike polymeric aggregates.

Since the geometry of the particles is similar over a wide range of polymer volume fraction, we will define in this paper the spatial organisation of these aggregates first in the dispersion and second in the film, at various water contents. After a brief description of the system and experimental conditions, we will describe the analysis of diluted solutions showing a large-scale aggregation and a long-range internal structure within the cylindrical motif. This picture will be then confirmed in the membrane form of Nafion, with the appearance of an orientation order between the colloidal particles that we analyze as a collection of bundles.

Experimental Section

Sample Preparation. Nafion 117 films, purchased from Aldrich and characterized by their equivalent weights, 1100 g/equiv, and thicknesses, 175 μm in a dry state, were used. The standard procedures were applied for the membrane preparation in term of cleaning; the membrane is soaked twice for 2 h in boiling HNO_3 1 M. Then, it is immersed for 1 h in boiling deionized water. Neutralization using lithium (Li^+), cesium (Cs^+) or tetramethylammonium (TMA^+) as counterions were performed in saturated chloride solution. For each case, the membrane is equilibrated for 2 days with a renewing of the solution, at least three times a day. Then the membrane is rinsed in pure water to remove the excess of salt. The swelling was obtained either controlling the water humidity in a homemade cell suitable for the required experiment or by swelling the film in a water-filled autoclave, at different temperatures above 100 °C. These hyperswollen membranes are kept in water. Nafion solutions in Li^+ or Cs^+ form are prepared according to the standard procedure.[11−14] The polymer volume fraction ϕ_p is determined by weighting the water uptake after drying and using 2.1 g/cm^3 for the polymer density. Some Nafion 115 and 112 membranes from du Pont de Nemours were also used, preparing in the same conditions as previously described, and no real differences in the data were observed.

Techniques. (a) Scattering. To probe the morphology, small-angle X-ray and neutron scattering (SAXS and SANS respectively) techniques were used. SANS were performed on the D22 spectrometer at the Laue-Langevin Institut (ILL, Grenoble, France). Two different configurations were used (i) $D_{s-d} = 2$ m and $\lambda = 6$ Å and (ii) $D_{s-d} = 17.6$ m and $\lambda = 10$ Å where D_{s-d} is the sample−detector distance and λ the incident wavelength. Preliminary experiments were performed at the Leon Brillouin Laboratory (LLB−CEA, Saclay, France). The samples immersed in aqueous solvent are placed in a closed quartz cells and maintained at room temperature. Neutrons were chosen to take advantage of the contrast variation method. To vary the scattering contrast between the polymer matrix and the solvent, the membrane samples were immersed in different mixtures of H_2O and D_2O. Moreover, the counterions were exchanged with TMA^+. This counterion will be used as a nontransient contrast agent; it is highly protonated and the protons of its methyl groups are not exchanged by D^+ like the H^+. Thus, it remains clearly *visible* in SANS with a scattering length density ($\rho_{TMA+} \approx -1$ cm^2/cm^3) different from those of D_2O ($\rho_{D_2O} \approx 6.34$ cm^2/cm^3) and the fluorinated parts ($\rho_F \approx 4.7$ cm^2/cm^3). Despite the methyl groups, this counterion is not a hydrophobic moiety and do not perturb the aqueous swelling of the membrane which is similar than in H^+ form.[58] Therefore, SANS combined with a contrast variation method is a suitable technique to determine the concentration distribution of the counterions in Nafion.

Some data were also obtained from small-angle X-ray studies (SAXS) performed on the ID02 beamline at the European Synchrotron Radiation Facility (ESRF, Grenoble, France).[59] Both pinhole SAXS and ultra-SAXS cameras were used in order to cover the widest range in scattering angle (with $\lambda = 1$ Å) and to analyze the very small angle intensity upturn with high resolution. In this article, the spectra are plotted as a function of the scattering vector q defined as followed: $q = 4\pi/\lambda \sin(\theta/2)$ with θ the scattering angle. Standard data corrections were applied depending on the neutron or X-ray scattering methods. The determination of the transmission factors as well as the sample thickness for the highly swollen samples was not so accurate; this explains why the scattering spectra are not given in absolute units (cm^{-1}). For ultra-small-angle X-ray scattering (USAXS) experiments performed on ID02, no folding operations were used since crossed channel-cut analyzers were mounted for the detection scanner.[59]

In parallel to the scattering experiments, two microscopy methods were used to probe the bulk and surface structure of Nafion film and dispersion.

(b) TEM. Sample for cryotransmission electron microscopy (TEM) experiments were obtained from a droplet of the Cs^+ form of Nafion solution, deposited onto a grid covered with commercial "lacey" carbon membranes (Pelco, USA) and quickly cooled into liquid ethane (−171 °C) in order to quench the polymer in a glassy water. Then, they were observed at −180 °C, under a weak dose exposure using a Phillips CM200 "cryo" microscope at 80 kV. Recorded on a photographic film (magnitude × 27500) and slightly out of the focal plane (Fresnel fringes are used for low contrast systems), the images present dark objects in a light background, the glassy water, in each cell of the carbon film. Nafion polymer is very sensitive to electron beam radiation, thus the exposure time vs the radiation rate was optimized to obtain good quality pictures as Cs^+ was used for enhancing the contrast. A series of solution concentrations were prepared in order to observe either individual or connected polymeric aggregates.

(c) AFM. Another way to probe the system in the real space is to use the atomic force microscopy (AFM) technique, a surface rather than a bulk characterization. Two kinds of samples were scanned. The first ones concern the dispersion study; the samples were prepared from a droplet of solution spread on a clean silicon wafer. The solvent is evaporated at room temperature so as to minimize the perturbation under these conditions and to analyze the surface as a bulk projection. The second type of samples surface are obtained from a cryo-fracture of a thick membrane under liquid nitrogen to image a surface that is the most representative of the internal structure. The AFM technique was used in a *soft contact mode* or more precisely using an intermittent-contact mode; for this purpose, the tip of the cantilever (NSC12/50 silicon cantilever from MikroMasch) interacts slightly with the material surface, once per oscillation, its vibration frequency being close to a resonance mode (300 kHz). The force applied by the tip is constant during the scanning using an electronic control loop. Then, utilizing a Digital Instrument dimension 3000 microscope, two types of signal are recorded: the height and phase variation as a function of the scanning position. The vertical and lateral resolutions depend on the force (or amplitude A) and tip radius (5−10 nm), respectively. For our study, we have fixed the ratio of the working amplitude over the intrinsic amplitude to 0.9 taking care of the surface and tip degradation.[60] In this regime, dark domains on the pictures corresponds to soft domains on which there is a large energy

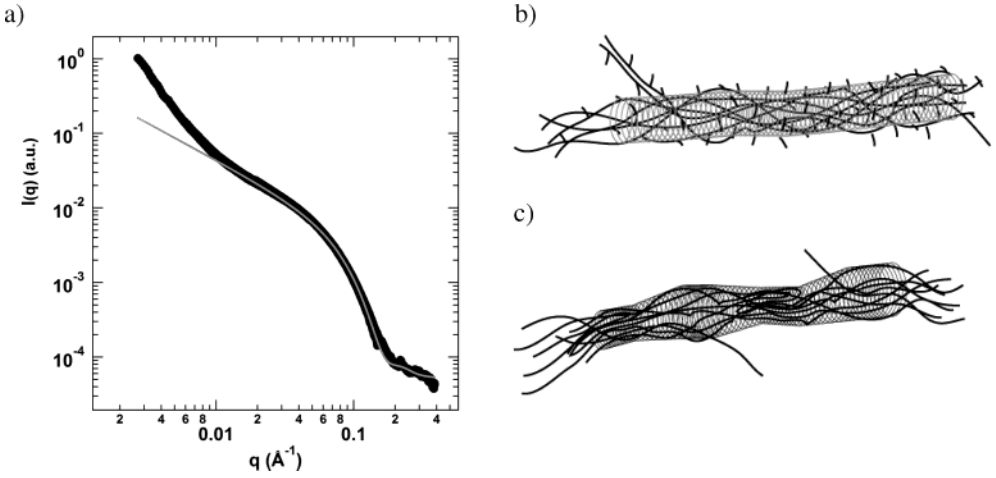

Figure 1. (a) SAXS spectrum of a diluted aqueous Li^+−Nafion 117 solution (log−log scale). The gray line plots the infinite cylinder theoretical form factor with a 40 Å diameter (and 20% in polydispersity). (b) Schematic view of an elongated polymeric aggregate that can be simulated by a rodlike form-factor, the sulfonated group being outside of the cylindrical core. (c) Schematic view of an elongated polymeric aggregate that can be drawn from microscopic observations and presenting an oscillation between more or less ordered phase of aligned polymer chains with the pendant chains toward the exterior. In both pictures, the gray spiral permits one to visualize in 3D the variation of the averaged diameter along the aggregate, either constant in case b or variable in case c.

dissipation of the cantilever and at the inverse, light domains corresponds to more rigid or elastic parts at the membrane surface.

Numerous pictures were recorded to check the reproducibility of our acquisition and to select images with a quite good quality in order to minimize the treatment like a flatten operation or other background subtraction. A power spectral density function proportional to the square of the Fourier transform of the 2D-topographic picture (from the Digital Instrument software) was applied to determine the roughness distribution function as a function of the inversed wavelength.

Results and Discussion

The first part is dedicated to the Nafion dispersion study presenting mainly the microscopy results in order to explain the intensity variation in the corresponding scattering spectra. In the second part, we will present results concerning hydrated membranes, still emphasizing the analogy between scattering and microscopy data.

Solution Characterization. In previous studies, Lopinnet et al. have shown that different fluorinated ionomer dispersions can be characterized as colloidal systems.[1,2] As an example, scattering data from a Nafion dispersion ($\phi_p = 0.3\%$) are plotted in Figure 1a; a log−log scale emphasizes the intensity variation at low q. We can observe three regimes as a function of q range: at large q (> 0.1 Å^{-1}) the scattering intensity decreases with oscillations around a q^{-4} power law and with a smooth minimum close to 0.16 Å^{-1}. A q^{-1} behavior in the intermediate regime is also observed, characteristic of elongated particles. Finally at low scattering wave vectors, a strong intensity upturn is visible; it could be analyzed considering either an aggregation between suspended particles or simply the presence of large coil-shaped particles made from the folding of very long cylindrical and flexible colloids.

The scattering curve analysis shows that a cylindrical form factor fits well with the data except at very low **q**-vectors. The diameter of these cylindrical aggregates varies from 30 to 50 Å depending on the solvent used. The consistent picture for these colloids corresponds to elongated particles made of packed and aligned backbone chains with the pendant sulfonated groups located at the periphery (see Figure 1b). At low concentration, these aggregates are more or less dispersed in the solvent.

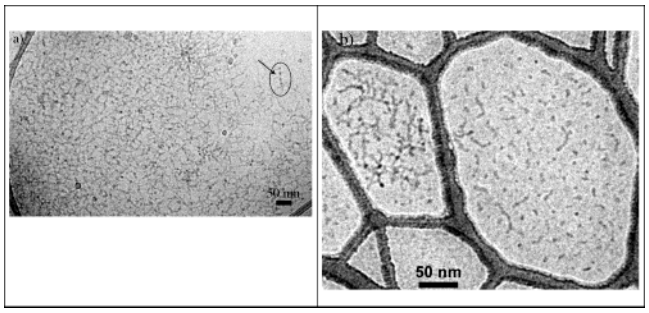

Figure 2. (a) Cryo-TEM picture of a Cs^+−Nafion 1100 solution, $\phi_p = 1\%$. (b) Cryo-TEM of Cs^+−Nafion 1100 solution, $\phi_p \approx 0.4\%$. The arrow in part a indicates a wormlike object with an oscillating contrast. The large scale "cell-wall" like structure is attributed to the supporting carbon membrane.

Up to now, no other evidence was presented to characterize this polymeric aggregation in the diluted suspension. For this reason, we present two different microscopy observations. The first one (see Figure 2a) corresponds to a transmission electron microscope image obtained from a droplet of Cs^+−Nafion 1100 dispersion. It is easy to discern a network of wormlike structure (dark fibrils) embedded in a vitreous ice (light background). This structure is relatively dense within it we can occasionally observe segmented objects. In Figure 2b, for which the native solution is more diluted, we observe independent wormlike objects with variable length. This distribution of lengths can be rationalized if we consider elongated polymeric aggregates oriented roughly perpendicular to the observation plane. Upon careful examination of the wormlike objects, we can distinguish some contrast variation along them, which is occasionally regular (see arrow in Figure 2a). They may be attributed to an electron-density variation due to a nonhomogeneous counterion Cs^+ distribution induced by a crystallinity wave along these objects.

After a bulk observation using TEM, another way is to observe a surface, which may mimic the internal structure of the dispersion. As explained in the Experi-

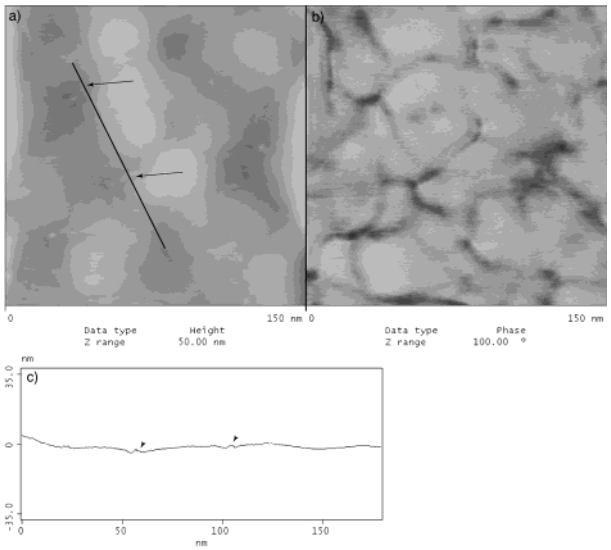

Figure 3. (a) AFM picture in topographic mode from a deposit of a Cs^+−Nafion 1100 solution on a silicon wafer. (b) Phase imaging. (c) Topographic profile corresponding to the drawing line-cut in part a, both arrows indicating the topological irregularities from the wormlike features.

mental Section, a thin film obtained from a cast-solution is probed using an AFM tip. An image is recorded at different radial positions from the center of the dried droplet and this is mainly in the central part that a structure is detected, as shown in Figure 3. On the topographic record of the film (see Figure 3a), we can distinguish a fibrilar network of topological irregularities on a wavy background. A line cut across the image shows that these *Z*-variations of the tip are weak (see arrows in Figure 3c). The phase image permits one to enhance the contrast of this structure at the surface of the substrate, as shown in Figure 3b, indicating a variation of the mechanical response along the cross section of this topological structure. This structure is quite similar to whose observed by cryo-TEM where the concentration of fibrilar objects is high. It looks like a wormlike network. The quality of the tip is important in resolving more detailed structure. The width of these fibrils, as estimated taking into account the convolution with the tip shape, is about 30−50 Å. These values are consistent with the values extracted from TEM and SAXS experiments if we consider that these topological variations correspond to polymer aggregates randomly deposited at the end of the evaporation process. However, it is difficult to extract a more accurate size and shape of the fibrils cross-section since the surface between them is a rough and soft polymer layer rather than a flat and hard silica surface. The wavy background observed on the topological image does not appear so homogeneous and the phase contrast reveals some mechanical response variation existing at a lower level from the surface. The noncontact method does not allow to highly resolve soft structures on a polymeric surface. Interestingly, as with TEM, the AFM images show a phase variation along these fibrillar objects. The origin of this variation is still unknown.

Nowadays, both microscopy and SAS are powerful technique to probe nanostructures. Yet the interpretation of the corresponding data remained subject to discussion when the system does not exhibit long-range position order or on the contrary corresponds to an isolated particle. Nevertheless their analyses lead to similar results and support the suggested picture of the Nafion colloids. The perfluorinated backbones are packed into an elongated aggregate as is sketched in Figure 1b, with the terminal ionic groups distributed at its surface. In an aqueous solvent, they behave as "macropolyelectrolytes". Moreover, the alignment of the Teflon-like backbones packed together is energetically favorable since the Teflon system is a rather crystalline material.[61] Clearly, the cylindrical geometry is not ideal since the length of the stretched pendant chain is about 10 Å. Thus, it does not allow one to place all the charges out of the aggregate with a diameter of about 30−40 Å. An elliptic or rectangular cross section of the particle may be preferred. However, the experimental resolution does not allow an accurate analysis of the oscillations in the Porod region of the scattering curves or the height profile of the AFM topographic records; it is currently impossible to differentiate between a rodlike and a ribbonlike shape.

We can also assume that some of the aligned chains interact more strongly within the aggregates and form crystallites as already suggested by Starkweather[62] and Tovbin et al.[38] This may be due to an inhomogeneous distribution of ionic groups along the polymer chains. Then, according to these microscopy observations, a slightly different picture of the elongated aggregates can be proposed. As drawn in Figure 1c, we can describe the electron density or the phase variation observed along the fibrils in TEM or in AFM respectively as, in a first approximation, an oscillation in size or in density (or both) along the cylinder axis. We will see further in the article that a model of a necklace particle which has been already considered for a low charge polyelectrolyte [65,66] allows one to describe the scattering intensity modulation in the Nafion film spectra as well.

Concerning the network organization, the observations in both AFM and TEM are similar. We observed a loose system made of connected or entangled rodlike aggregates rather than a dispersion of coiled and micrometric particles made of very long fibrils. This agrees with the picture of Cirkel et al.[49] Indeed, when the Nafion suspension is concentrated and viscous, it forms a network of elongated aggregates as suggested in ref 49. They can thus explain the rheological and impedance measurements during the gelling process of Nafion solution.[50] Moreover, the ability to solubilize carbon nanotubes in the presence of the Nafion[65] could be also considered within this type of picture, optimizing their association.

Film Characterization. It is well-known that the Nafion membrane structure is characterized by a nanophase separation between hydrophilic and hydrophobic domains.[20−22] Utilizing SANS with a partially deuterated solvent and a highly protonated counterion such as TMA^+, we have previously demonstrated the counterions condensation at the interface of these domains.[66] Furthermore, we have shown that the scattering curves from highly swollen membranes could be to some extent modeled as a core−shell cylindrical structure with a polymeric core surrounded with a counterions shell. We found that the core diameter of the scattering particles is slightly smaller than that determined in colloidal dispersions.

As mentioned in the Introduction, the aim of the paper is to determine the spatial organisation of these aggregates, first at small scales, within few tens of nanometers, and second at large scale in the submicrometer range.

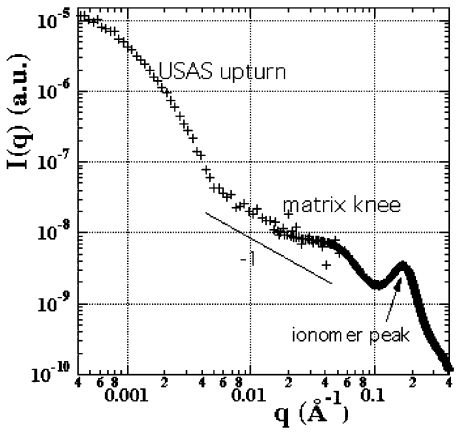

Figure 4. Typical scattering spectrum of water swollen Nafion 1100 obtained using X-rays and over a large scale of wave vectors.

(a) Small Scales. The scattering data analysis of nondiluted systems is complex in the absence of Bragg peaks due to a lack of periodicity. This problem is more critical when the scattering entities are anisotropic—rodlike in our case. Yet, it was recently shown that SAS curves for hydrated Nafion membranes are similar over a large polymer volume fraction range, corresponding to different swelling states.[3] A typical spectrum is presented in Figure 4.

This latter observation will permit us to analyze the scattering curves as was performed for the highly swollen membrane. Moreover, an assumption of a local correlation in orientation, depicted as a bundle of elongated aggregates (see Figure 10a), can be proposed and checked afterward. In other words, the collection of aggregates can be analyzed as a powder of monodomains of relatively oriented particles. Thereby we can evaluate the scattering data as a product of a structure factor $S(\vec{q})$ with the form factor $P(\vec{q})$ of a rodlike particle, in the case of Nafion. This means that we can separate analytically the inter- and intraparticle contributions to the scattering intensity.

This type of approach is usually valid when the scattering objects are spherical. However, we can assume that it is still valid if we consider that, within one domain, the correlation function does not depend on the mutual orientation of the scattering particles (no orientation fluctuations). It depends only on their positions, and consequently the averaging could be applied only at the domains scale. This analysis was applied already on scattering data from liquid crystal phases like nematic, lamellar or hexagonal phases.[67,68] Then the scattering intensity $I(\vec{q})$ of one monodomain which is in general proportional to $|\sum_{i=1}^{N} e^{i\vec{q}.\vec{R}_i(t)} \int_i \mathrm{d}\vec{r} e^{i\vec{q}.\vec{r}} f_i(\vec{r},t)|^2$ with N is the number of particles, each of them being at position $R_i(t)$ and f_i a factor equal to 0 or 1 and characterizing the particle at the time t. This expression can be simplified to $I(\vec{q}) \propto NV^2S(\vec{q})P(\vec{q})$, V being the volume of the particle. Now, if we consider the Nafion film in TMA^+ form, the scattering length density ρ (SLD) variation at the interface between the solvent and the aggregates has to be described using a two-step function with ρ_{core}, $\rho_{solvent}$, and ρ_{shell}.[66] If we define L, R, and e as the length, the radius of the cylinders, and the shell thickness, respectively, and φ the angle between $\vec{q}$ and the orientation axis, the form factor can be written as[3,69]

$$P(\vec{q}) \propto \left[A(q,\varphi,L,R+e) + \frac{\rho_{core}-\rho_{shell}}{\rho_{shell}-\rho_{solvent}} \cdot \frac{V(R)}{V(R+e)} A(q,\varphi,L,R)\right]^2$$

with

$$A(q,\varphi,L,R) = 2\frac{\sin(qL/2\cos\varphi)}{qL/2\cos\varphi}\frac{J_1(qR\sin\varphi)}{qR\sin\varphi}$$

whereas $S(\vec{q})$ contributes to the scattering only in the direction perpendicular to the cylinders axis. A so-called powder averaging can be performed by integration over the orientation angles φ. The form factor leads to a new expression of $P'(q) = 2\pi\int_0^\pi P(\vec{q}) \sin\varphi \, \mathrm{d}\varphi$. $S(\vec{q})$ becomes $S'(q)$ and then contributes to the scattering in all the directions.

For a given polymer volume fraction, the form factor of the core−shell aggregate will change by varying the solvent SLD using different mixtures of H_2O and D_2O whereas the structure factor will be identical. Indeed it has been shown that the solvent deuteration does not change the ionomer peak position.[70] Then, the SANS data analysis can be performed as in reference,[66] by dividing the different spectra obtained for various H_2O/D_2O mixtures with those of the sample in pure water. This operation allows us to eliminate the structural component $S'(q)$ that we do not know how to model. Figure 5 presents the division of these scattering curves for various polymeric volume fractions.

Thus, the full curves correspond to the theoretical adjustment with the ratio

$$\frac{I_{solvent}}{I_{H_2O}} = K\frac{\int_0^\pi \left[A(q,\varphi,L,R+e) + \frac{\rho_{core}-\rho_{shell}}{\rho_{shell}-\rho_{solvent}}\cdot\frac{V(R)}{V(R+e)}A(q,\varphi,L,R)\right]^2 \sin\varphi \, \mathrm{d}\varphi}{\int_0^\pi \left[A(q,\varphi,L,R+e) + \frac{\rho_{core}-\rho_{shell}}{\rho_{shell}-\rho_{H_2O}}\cdot\frac{V(R)}{V(R+e)}A(q,\varphi,L,R)\right]^2 \sin\varphi \, \mathrm{d}\varphi}$$

with the following parameters R, e, and ρ_{core}. K is a scaling constant and L is supposed to be very large (>1000 Å). These parameters are summarized in Table 1 for four polymer volume fractions taking into account a Gaussian distribution on R of 20%:

The adjustment of the experimental curves is quite good over practically two decades in **q**-vectors. The amplitudes and positions of the intensity oscillations are well described whatever the degree of swelling. However, some mismatches exist at low angles for the high ϕ_p membranes and at large angle for the low ϕ_p membranes. It is important to point out that, for a given ϕ_p, we obtain a relationship between the SLD of the core and the ionic shell as a function of the contrast variation, the SLD for the solvent (considering all the counterions as condensed) being calculated. Taking into account a monotonic variation of this relationship, ρ_{core} is determined with a quite good accuracy.[33] Moreover, if e is let free for the adjustment, the radius of the cylindrical core are close (less than 10%) to those indicated in the Table 1. Then, fixing e to the value determined for the most swollen sample—Naf−Φ_{16}—we obtained an effective core's radius R, which decreases as a function of ϕ_p. This variation, which is not negligible, is surprising and cannot be taken into account considering only an ionic shell thickness variation. We

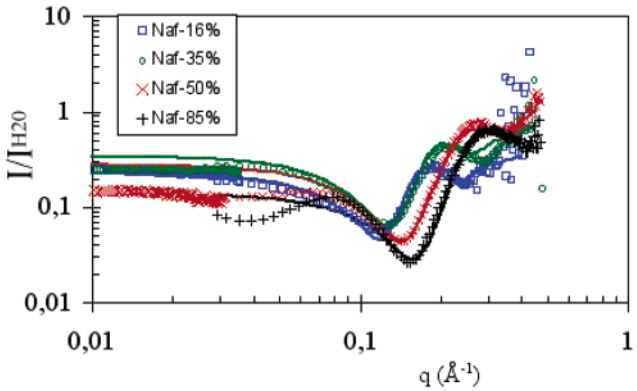

Figure 5. Spectra of Nafion membranes neutralized by $N(CH_3)_4^+$ in D_2O and normalized by the spectrum of Nafion membrane in pure H_2O for four different polymer concentrations ϕ_p (or degree of swelling) 16, 35, 50 and 85%. The low angle part is missing for $\phi_p = 0.85$. Full curves correspond to model of the form factors division considering infinite shell-cylinders.

Table 1. ϕ_p, the Polymer Volume Fraction[a]

sample	ϕ_p	R_{cyl} (Å)	e (Å)	ρ_{core} ($\times 10^{10}$ cm/cm^3)
Naf−Φ_{16}	∼0.16	21	4.3	4.7
Naf−Φ_{35}	∼0.35	17.7	4.3	4.7
Naf−Φ_{50}	∼0.5	14.6	4.3	4.7
Naf−Φ_{80}	∼0.8	13.5	4.3	4.7

[a] The fit parameters are R the cylindrical radius, e the ion shell thickness, and ρ_{core} the scattering density of the cylinder core. L is chosen larger than 1000 Å.

did not taken into account that the conformation or extension of the pendant chains and the polymer backbones packing as well can vary as a function of the water content and the thermal treatments; we could then consider a size variation on the apparent diameter extracted from the scattering data. However, we have used for this analysis a minimum number of parameters; thereby, if we consider a different radial density profile for the aggregate, other parameters have to be introduced, increasing the number of options that will clearly improve the data adjustment without being more convincing on the real shape of the aggregates. The mismatches observed at large angles of scattering (below 0.3 Å^{-1}) for the swollen membranes could be explained by some difficulties observed in subtracting accurately the incoherent background from water, before the spectra division. This could also suggest that the interface SLD variation between the polymeric core of the aggregates and the surrounding solvent is slightly smoother than in a two-step model. For membranes with low water content, the differences between the theoretical adjustments and experimental data, at low angles, can originate from the crystalline parts or size variation along the particle as we suggested in the previous section. We have always considered a homogeneous cylinder along its axis as a form factor for the scattering motif. In the appendix, we treat two simple modulations along the cylindrical core, a diameter and a SLD sinusoidal variation that might be an explanation of the intensity modulation in this q range. In the same way, we can also consider that the hydration shell around the aggregates is not homogeneous at low water content; this might be also an explanation for the differences observed at low **q**-vectors (below 6×10^{-2} Å^{-1}) and the radius R variation as a function of ϕ. However, the first and important result of our analysis

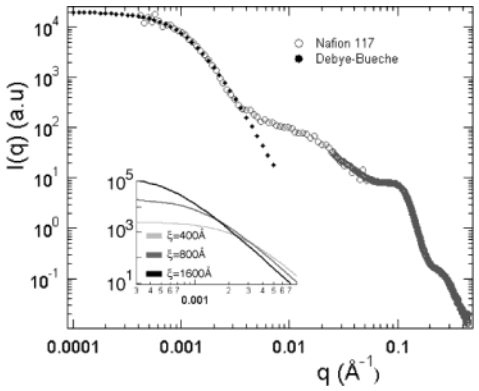

Figure 6. Adjustment of Debye−Bueche scattering model (full line) on the low-q part of the small angle scattering spectrum from a Nafion 117 membrane in water and exchanged with Lithium counterions (dotted line). The correlation length in the fit is equal to 800 Å. Inset: Plots of the theoretical scattering intensity using a Debye−Bueche description for three different correlation lengths.

concerns the validation of our assumption describing the scattering intensity expression in term of a product of a form and a structure factor. Second, we have shown in previous papers that the swelling process to dilute these aggregates can be analyzed with a 1D followed by a 2D dilution law.[3,39] There are two conditions, perhaps not sufficient but necessary to be able to consider a local correlation in orientation between the aggregates. This local orientation can be depicted as bundles of fibrils, the main axis of this bundles being randomly distributed in space. Concerning the real shape of the aggregates, the swelling law suggests a lamellar system (already considered by different authors[36,38]) with a uniaxial symmetry that could be associated with a ribbonlike motif.

Then the last point concerns the characteristic size of this correlation, which can be determined using USAXS and AFM techniques.

(b) Large Scales. The strong intensity upturn that can be observed in the scattering spectra, using a suitable technique (usually a Bonse and Hart camera), was already analyzed on Nafion and other ionomer films[3,24,40−45] in term of large scales density fluctuations. Two explanations have been proposed. The first one is based on the assumption of an inhomogeneous distribution of ionic groups while the second takes in account an inhomogeneous hydration of the ionic groups related to an inhomogeneous distribution of crystallinity.

A suitable scattering model to analyze these inhomogeneities is the Debye−Bueche model,[71,72] which assumes an isotropic and exponential decay of the electron-density correlation. The corresponding scattering intensity description can be written as follows:

$$I(q) = \frac{A\xi^3}{(1 + q^2\xi^2)^2}$$

with ξ a correlation length and A a scaling constant which depends on the system. This model allows one to describe well this intensity upturn, and several correlation lengths were determined from few hundred up to thousands of nanometers depending on the system. The high resolution of our experimental setup allows us to get data at very low q values and to really detect the level-off of the intensity upturn, which permits a more accurate analysis. Figure 6 presents the experimental

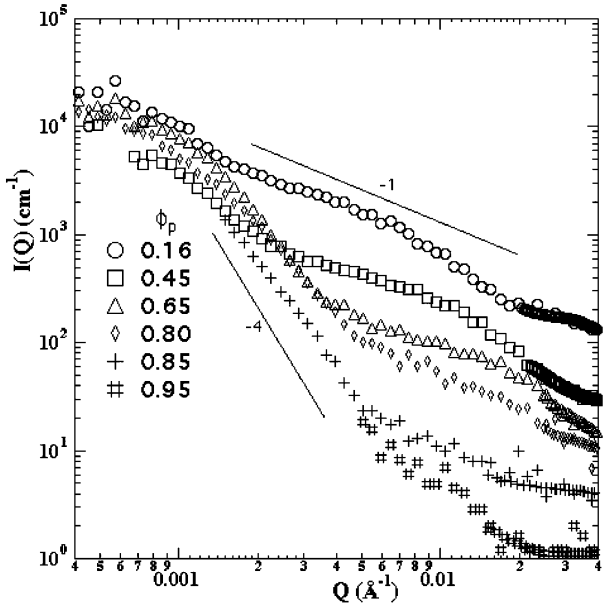

Figure 7. USAXS upturn from Nafion 1100 as a function of the water content or polymer volume fraction ϕ_p.

data and their adjustment using the Debye−Bueche model. A correlation length of 800 Å can be determined for this example, a water swollen Li^+-form Nafion 117. This value varies slightly from one sample to another and we found values of the same order for other fluorinated systems like DOW or Aciplex membrane. In the inset of Figure 6, the scattering intensities are plotted as expressed above for three different correlation lengths.

This upturn was studied as a function of the water content in membranes from dry up to its highly swollen state (see Figure 7). At a low water content, when the membrane is equilibrated with humid air, the saturation of the scattering upturn is not observable because of the weak signal compared to the intrinsic camera background. For relative humidities below 70%, this upturn is even not detectable at all. At the opposite, when the membrane is in water, this intensity upturn is strong enough to be resolved but becomes less and less discernible for the high swelling degree. This is due to a simultaneous enhancement of the intensity level of scattering part at larger q. The curvature of this intensity upturn, which characterizes the correlation loss, seems to not change drastically as a function of the polymer volume fraction as we can see in Figure 7.

From contrast variation measurements, we observed that the square root of the scaling constant vary linearly with the fraction of deuterated water and cancel out at a fraction of about 70%. This corresponds to the contrast matching of the fluorinated polymer and indicates that the heterogeneity observed at large scales comes mainly from an inhomogeneous hydration of the membrane at the thousand angstroms scale.

As performed on the Nafion dispersions, the AFM technique was used to detect these large scales density fluctuation and more especially their characteristic size. Figure 8 presents two AFM topographic images: the left-hand side image corresponds to a scan on the external surface of a Nafion membrane whereas the right-hand side corresponds to a scan on a surface obtained after a cryofracture of the membrane. As explained in the Experimental Section, this latter surface should mimic the bulk structure of the membrane and this is mainly on these sections that we focalized our microscopy work. This type of rough surface presented in Figure 8b has already been observed in previous studies of Nafion.[53,60,73−75] The Nafion surface response looks like modulated at the submicrometer scale whatever the lateral scan direction and its image is reproducible.

We have analyzed more quantitatively this modulation applying the azymuthal averaged on the square 2D-Fourier transform of the phase image shown in Figure 9a. For this purpose we used a mathematical 2D-transformation from Digital Instrument software and we obtained a topographic intensity variation as a function of an inverse wavelength, plotted in Figure 9b. These data sets are characterized by a frequency threshold below which the signal is getting saturated. We can use the same exponential correlation function than for the Debye−Bueche model, $\exp(-r/\xi)$, on which we apply a 2D Fourier transform:

$$J = \int_0^{\infty}\int_0^{\pi} e^{-r/\xi} e^{-i\vec{q}.\vec{r}}\, r\, dr\, d\theta$$

The experimental data can be fitted using this expression with a correlation length ξ, which is 600 Å for this example (see Figure 9b).

It appears that this characteristic length is of the same order of the correlation length extracted from USAXS experiments. However the environmental conditions are not really equivalent, the water content being not similar. We succeeded in performing AFM scans in relative humidity controlled conditions up to 55%, but that is not high enough to compare the results with those of scattering. We did not observe some drastic changes of the surface modulation by varying the relative humidity around the membrane from 16 up to 55% of RH. We expect to observe an effect either at very low content of water (ϕ_p > 90%) between a really dry state and the first step of the water molecules sorption or at larger water content when the membrane is equilibrated around 100% of RH. Improvements have to be made to perform AFM scans close to 0 and 100% of RH and in liquid water. Nevertheless we can consider that the large-scale fluctuations observed using scattering techniques can be related to the large scale mechanical inhomogeneities detected using the AFM technique.

Intuitively, we associate this large-scale characteristic length, which can be determined in microscopy and scattering techniques, to a correlation length in orientation between the elongated polymeric aggregates. To have a schematic view of the Nafion structure, we can represent it as a powder of domains in which these aggregates are relatively oriented (see Figure 10A). At a low water content (ϕ_p>85%) the aggregates are totally or partially collapsed (see Figure 10B1); If the hydration is not totally homogeneous around the particles, the SLD variation at that scale do not permit to reveal the q^{-1} power law regime in the scattering curves. It is mainly the one-dimensional SLD modulation along the aggregates, which we suggest to be correlated to the crystallinity, that is detectable and that appear in the scattering curves. When the water content is increasing, the aggregates in their bundle start to become dissociated, keeping an orientation order (see Figure 10B2). The ionomer peak characterizes their mean distances and shifts to a lower angle as the water content increases. The q^{-1} regime is more clearly visible. The

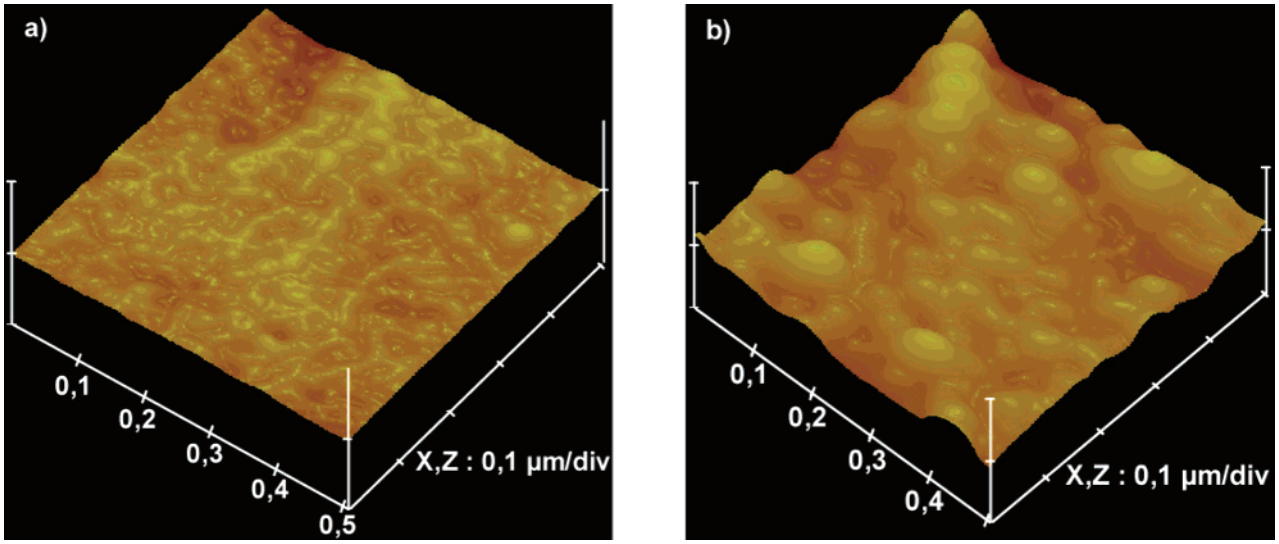

Figure 8. AFM topographic images of a Nafion 1100 membrane (a) at the surface of the native film and (b) at the surface of a cross section of the membrane obtained after a cryofracture. The scales (0.5 × 0.5 μm^2) are the same for both images.

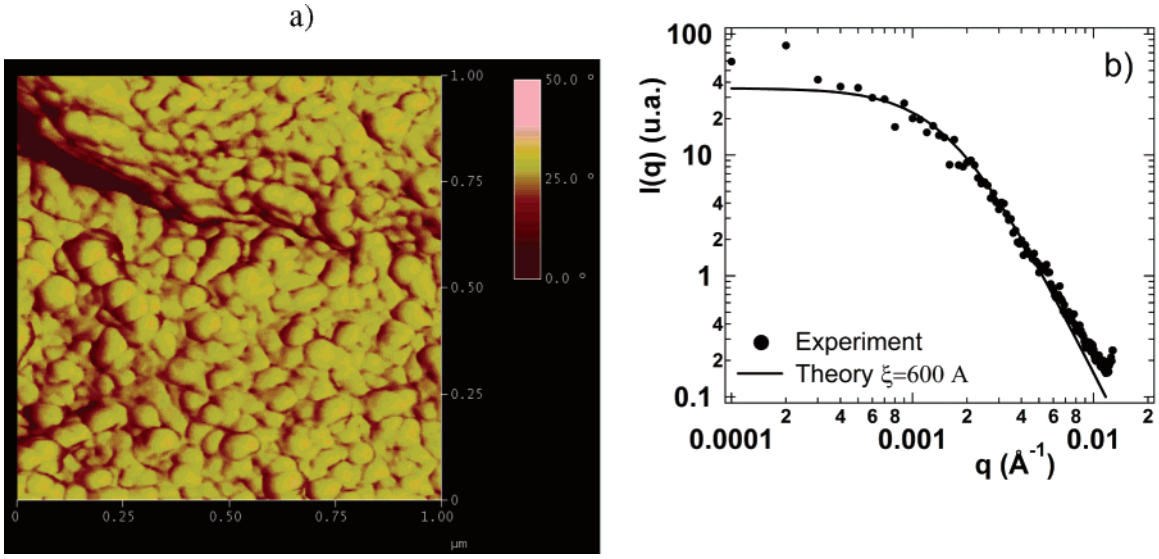

Figure 9. (a) Analysis of the AFM phase image on a Nafion 117 surface at room humidity. (b) Comparison between the azymuthal averaged square 2D Fourier transform of the phase image (full line) and the 2D Fourier transform of an exponential correlation function as used in the Debye−Bueche model to analyze the ultralow angle scattering spectrum (dotted line). A characteristic length of the order of 600 Å is determined for the adjustment.

number of individual scatters increases that could explain the enhancement of the scattering intensity level observed in Figure 7. The bundle picture characterizes a local orientation order, which is lost over the order of 500−1000 Å depending on the water content. In a first approximation, it can be depicted as a powder structure; the difference in orientation between the domains gives the necessary contrast to observe them in scattering or in microscopy. The swelling has to be understood as a one- or two-dimensional disentanglement rather than a pure colloidal dilution. The temperature treatment used to increase the swelling of the membrane brings the required energy to physically separate the aggregates until their complete dispersion. This dissociation is partial and continuous over the whole swelling process.[80] Although the real description should be more complex, our assumption that the Nafion membrane is composed of an assembly of bundles of fibrils (see Figure 10A) allows us to analyze the anisotropic scattering spectra observed when a strain is applied on the membrane[76,77] and the optical properties of birefringence as well.[31,78]

We do not have any information on the total length of the aggregates to quantify this analysis, but we have observed that at a low volume fraction of polymer the system has the tendency to form a network, an organization that prevents this determination. We have shown that, using AFM, it was difficult to resolve the individual aggregates packed into the bundles. However, a recent analysis[79] using a scanning tunneling microscopy permits to extract the bundles of cylindrical polymeric aggregates from a similar perfluorosulfonated system from DOW Chemical. Taking advantage of the presence of charges in the system, this is perhaps a more suitable technique to analyze in the real space this fibrillar morphology.

We would like to emphasize that if we compare the Gierke model with our structural proposal, few differences exist at the nanometer scale. Observing the bundle structure through a plan crossing the ag-

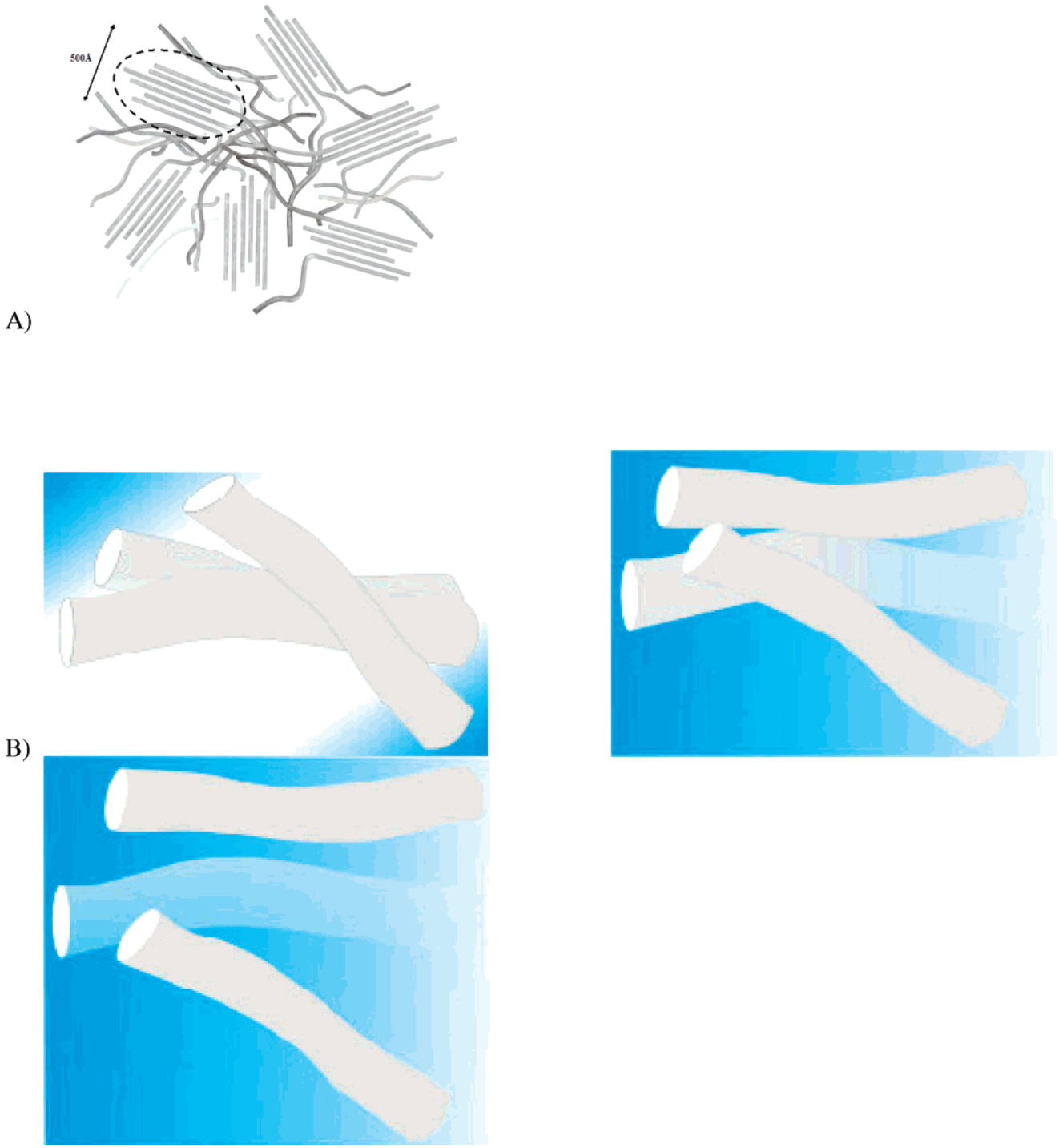

Figure 10. (A) Schematic view of correlated polymeric aggregates domains—a bundle, the position and orientation order inside a bundle being characterized by the ionomer peak and the correlation length (between 50 and 100 nm) characterized by the USAS upturn. (B) Schematic view of a nanoscopic swelling between three aggregates and inside a bundle over a large water content variation (from almost dry membrane up to diluted solution).

gregates, we can represent the hydrated Nafion as a 2D micellar structure, with disks of ions and water connected by channels. However, the difference comes from the fact that a polymer chain organization exists in the third dimension, which has to be taken into account at the structural point of view to analyze the macroscopic transport and mechanical properties.

Finally, from scattering and microscopic techniques, we were able to detect large-scale density domains, but we were unable to extract information on the aggregate's conformation between these mesoscopic domains. We have determined a correlation length characterizing an orientation correlation, but it will be interesting to quantify this disorder, which certainly have an effect on the transport and mechanical properties of the film.

Conclusion

Combining SANS and contrast variation with a highly protonated counterion as a third scatter, which is condensed at the interface between the scattering object and the solvent, we have demonstrated (i) that elongated polymeric aggregates present in the Nafion suspension are also the basic entity in the Nafion mem-

brane even at low water content and (ii) that a local orientation of these aggregates can be considered and is characterized by a correlation length about few hundred of nanometers. The intrinsic anisotropic structure due to the alignment of the polymer chain were already proposed; however, we demonstrate that an analysis over a large variation of length and water swelling becomes really necessary if we want to answer without ambiguity the question of ion and water distribution in these ionomer systems. In the case of Nafion, the water is not confined in spherical cavities but between fibrillar objects and becomes as a function of the hydration rate a continuous medium around an intrinsic anisotropic structure. Our analysis is valid and powerful to characterize complex structures like Nafion, and simultaneous studies in real and Fourier spaces allow us to give a more coherent structural model of this ionomer system. It should be applied to characterize alternative ion conducting membranes.

Acknowledgment. We are grateful to J. L. Putaux for his expertise in TEM and providing to us the best quality in the cryo-TEM images in Nafion solution. It is a pleasure to thank F. Rieutord for our initiation into the AFM techniques and for his fruitful discussion and G. Albert for his technical help for building the homemade cells. L.R. thanks the CEA for his financial support (MRT). ESRF and ILL generously allocated beamtime, and I. Grillo and P. Panine are acknowledged for help with operation of the D11 spectrometer and ID2 beamline, respectively.

Appendix

From the AFM phase variation observed along the polymeric aggregates and from the low-q mismatches in the scattered intensities divisions, we can express the existence of a structural modulation within and along the axis of the cylinders. Two simple approaches are considered: a ρ_{core} and a radius sinusoidal variation as a function of the length L of the elongated aggregate. The former, the ρ-model, corresponds to electron density variation along the tube keeping the diameter constant. The latter, called the R-model, corresponds to a radius variation along the tube, keeping the density constant. Then, can we fit the matrix knee observed in the q^{-1} scattering regime and the general shape of the scattering curve as well, with the corresponding form factors P1 and P2 characterizing the intraparticle correlation?

We can write the corresponding expressions, including two new parameters, λ and b ($0 \le b < 1$), the period and the amplitude of the modulation respectively around the averaged radius R^0 or the SLD ρ^0_{core} depending on the model.

The scattering amplitude from an homogeneous cylinder of length L and radius R is well-known and is written

$$A(\vec{q}) = \int_V \rho e^{i\vec{q},\vec{r}}\, d\vec{r}$$

with r the scattering density and V the volume of the particle.

Developing this expression and using the Bessel function integral properties, we obtain

$$A(\vec{q}) = [\int_{-L/2}^{L/2} e^{iqz\cos(\varphi)}\, dz][\int_0^R r\, dr \int_0^{2\pi} e^{iqr\sin(\varphi)\cos(\theta)}\, d\theta]$$

Now, if we consider, first, a sinusoidal inhomogeneity in the scattering density along the z axis of the cylinder under the form: $\rho(z) = \rho_0(1 + (1 - b)\cos(2\pi/\lambda\, z))$ with b the amplitude of the oscillations ($0 \le b < 1$) and λ the corresponding period, the scattering amplitude can be decomposed in different terms:

$$A_\rho(\vec{q}) = \left[\int_{-L/2}^{L/2} \rho_0 e^{iqz\cos(\varphi)}\, dz + \int_{-L/2}^{L/2} \rho_0(1 - b) \times \cos\left(\frac{2\pi}{\lambda} z\right) e^{iqz\cos(\varphi)}\, dz\right]\left[\int_0^R r\, dr \int_0^{2\pi} e^{iqr\sin(\varphi)\cos(\theta)}\, d\theta\right]$$

Developing this, we obtain

$$A_\rho(\vec{q}) = 2\frac{J_1(qR\sin\varphi)}{qR\sin\varphi} \times \begin{pmatrix} \sin c(qL/2\cos\varphi) \\ -\frac{(1-b)}{2}[\sin c((2\pi/\lambda + q\cos\varphi)(L/2)) + \\ \sin c((q\cos\varphi - 2\pi/\lambda)(L/2))] \end{pmatrix}$$

The second approach is to consider a sinusoidal inhomogeneity characterized by a radius variation:

$$R(z) = R_0\left(1 + (1 - b)\cos\left(\frac{2\pi}{\lambda} z\right)\right)$$

Then

$$A_R(\vec{q}) = \int_{-L/2}^{L/2} e^{iqz\cos(\varphi)}\, dz \int_0^{R(z)} r\, dr \int_0^{2\pi} e^{iqr\sin(\varphi)\cos(\theta)}\, d\theta$$

Now the development has to take into account the variation of R in the integration limits:

$$A_R(\vec{q}) = 4\pi {R_0}^2 \int_0^{L/2}\left(1 + (1 - b)\cos\left(\frac{2\pi}{\lambda} z\right)\right) \times \frac{J_1\left(qR_0\sin(\varphi)\left(1 + (1 - b)\cos\left(\frac{2\pi}{\lambda} z\right)\right)\right)}{qR_0\sin(\varphi)} \times \cos(qz\cos(\varphi))\, dz$$

For both approaches, the corresponding form factor is proportional the square of the scattering amplitude, and if we take into account the spatial average, then

$$P(q) \propto 2\pi {\rho_0}^2 \int_0^\pi |A(\vec{q})|^2 \sin\varphi\, d\varphi$$

using $A_R(\vec{q})$ or $A_\rho(\vec{q})$.

In both models, no counterion shell will be taken into account in order to simplify the equations. In Figure 11 are plotted P1 and P2 with different values of λ and b and for a given R^0 or ρ^0_{core} as indicated in the figure caption. The theoretical curves are folded with a Gaussian function characterizing a distribution of the period with an intrinsic width $\Delta\lambda$ equal to 10% of λ. For sake of clarity the curves are scaled with an arbitrary constant so as not to overlap.

The first result concerns the appearance in both cases of a local maximum in the q^{-1} regime, which is broadening by the distribution. Varying the period from 150 up to 1000 Å depending on the water content, we can reproduced quite well the experimental data in this q range. The second result concerns the smoothing of the oscillations in the Porod regime (large q range) in the

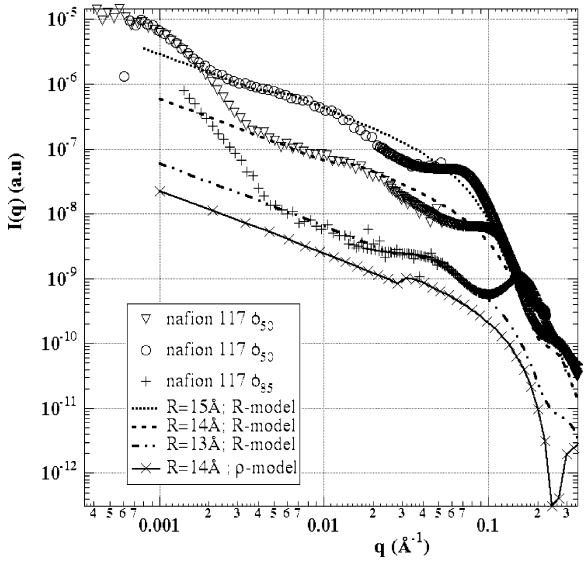

Figure 11. Comparison between experimental scattering data and z-modulated form factor of cylindrical particles as described in appendix. The dotted line curves correspond to the R-model with different sets of parameters (R = 15 Å, ΔR = 0.5, λ = 1200, $\Delta\lambda$ = 0.1; R = 14 Å, ΔR = 0.5, λ = 500, $\Delta\lambda$ = 0.1; R = 13 Å, ΔR = 0.5, λ = 150, $\Delta\lambda$ = 0.1). The black and full curve corresponds to the ρ-model with R = 14 Å, $\Delta\rho$ = 0.5, λ = 150, and $\Delta\lambda$ = 0.1. The data points are experimental data for three different polymer volume fractions and are plotted with an arbitrary scale compared to the form factor plots to be used as a guide for the eyes.

case of the R-model. As a matter of fact, a radius polydispersity is intrinsically contained into the model. Now, if we analyze the parameters, we first deduce, from the ρ-model, a b value larger than 1 in order to match the experimental amplitude of the matrix knee; it has no physical meaning by definition. On the other hand, the b value extracted from the R-model, around 0.4−0.5, gives the right amplitude and broadness of the matrix knee in the scattering profiles. These values are perhaps slightly too large but combining both effects, which looks like reasonable (an effect of size variation should be naturally related to a scattering density variation), we can expect to analyze successfully the data. We have to keep in mind that we considered a simple sinusoidal function for the modulation, which should be certainly more complex if it is related to the crystallinity distribution. An experimental work is necessary to really analyze the degree of crystallinity as a function of ϕ_p and then to quantify this modulation. However, with a simple assumption based on the microscopy observations, we can reproduce the matrix knee of the Nafion scattering curves.

References and Notes

(1) Lopinnet, B.; Gebel, G. *Langmuir* **1998**, *14*, 1977.
(2) Loppinet, B.; Gebel, G.; Williams, C. E. *J. Phys. Chem. B* **1997**, *101*, 1884.
(3) Rubatat, L.; Rollet, A.-L.; G. Gebel, G.; Diat, O. *Macromolecules* **2002**, *35*, 4050.
(4) Heitner-Wirgin, C. *J. Membr. Sci.* **1996**, *120*, 1.
(5) Savadogo, O. *J. New Mater. Electrochem. Syst.* **1998**, *1*, 47.
(6) Jurado, J.; R.; Colomer, M. T. *Chem. Ind.* **2002**, *56*, 264.
(7) Wakizoe, M.; A.; V. O.; Srinivasan, S. *Electrochim. Acta* **1995**, *40*, 335.
(8) Bahar, B.; Hobson, A. R.; Kolde, J. A.; US Patent No. 5,599,614.
(9) Kato, H.; US Patent No. 6,054,230.
(10) Costmagna, P.; Srinivasan, S. *J. Power Sources* **2001**, *102*, 253.
(11) Kreuer, K. D. *J. Membr. Sci.* **2001**, *185*, 29.
(12) Besse, S.; Capron, P.; Diat, O. *J. New Mater. Electrochem Syst.* **2002**, *5*, 109.
(13) Jannasch, P. *Curr. Opin. Colloid Interface Sci.* **2003**, *8*, 96.
(14) Grot, W. G.; Chadds, C. European Patent 1982, 0 066 369.
(15) Martin, C. R.; Rhoades, T. A.; Fergusson, J. A. *Anal. Chem.* **1984**, *54*, 1639.
(16) Gamburzev, S.; Appleby, A. J. *J. Power Sources* **2002**, *107*, 5.
(17) Zawodzinski, T. A.; Derouin, C.; Radzinski, S.; Sherman, R.; J.; Smith, V. T.; Springer, T. E.; Gottesfeld, S. *J. Electrochem. Soc.* **1993**, *140*, 1041.
(18) Eikerling, M.; Kornyshev, A. A.; Stimming, U. *J. Phys. Chem. B* **1997**, 101**,** 10807.
(19) Eisenberg, A. *Macromolecules* **1970**, *3*, 147.
(20) Gierke, T. D.; Hsu, W. Y.; Heisenberg, A.; Yeager, H. L. E. *ACS Symposium Series*; American Chemical Society: Washington, DC, 1982.
(21) Roche, E. J.; Pineri, M.; Duplessix, R.; Levelut, A. M. *J. Polym. Sci., Polym. Phys. Ed.* **1981**, *19*, 1.
(22) Fujimura, M.; Hashimoto, T.; Kawai, H. *Macromolecules* **1982**, *15*, 136.
(23) Pineri, M.; Duplessix, R.; Volino, F. *Perfluorinated Ionomer Membranes*; ACS Symposium Series C180; American Chemical Society: 1982, p 249.
(24) Yarusso, D. J.; Cooper, S. L. *Macromolecules* **1983**, *16*, 1871.
(25) Mauritz, K. A.; Rogers, C. E. *Macromolecules* **1985**, *18*, 483.
(26) Dreyfus, B. In *Simple Considerations on the Morphology of Ionomers*; Eisenberg, M. P. A., Ed.; D. Riedel Publishing Company: Dordrecht, The Netherlands, 1987.
(27) Orfino, F. P.; Holdcroft, S. *J. New Mater. Electrochem. Syst.* **2000**, *3*, 285.
(28) Gierke, T. D.; Munn, G. E.; Wilson, F. C. *J. Polym. Sci.; Polym. Phys. Ed.* **1981**, *19*, 1687.
(29) Gardner, C. L.; Anantaranam, A. V. *J. Electroanal. Chem.* **1995**, *395*, 67.
(30) Fontanella, J. J.; McLin, M. G.; Wintersgill, M. C.; Calame, J. P.; Greenbaum, S. G. *Solid State Ionics* **1993**, *66*, 1.
(31) Van der Heijden, Bouzenad, F.; Diat, O. *J. Polym. Sci.; Polym. Phys. Ed.* **2004**, *42*, 2857.
(32) Wodski, R.; Narebska, A.; Nioch, W. K. *J. Appl. Polym. Sci.* **1985**, *30*, 769.
(33) Cwirko, E. H.; Carbonell, R. G. *J. Membr. Sci.* **1992**, *67*, 227.
(34) Haubold, H. G.; Vad, T.; Jungbluth, H.; Hiller, P. *Electrochim. Acta* **2001**, *46*, 1559.
(35) Falk, M. *Can. J. Chem.* **1980**, *58*, 1495.
(36) Litt, M. H. *Polym. Prepr. (Am. Chem. Soc., Div. Polym. Chem.)* **1997**, *38* (1), B0.
(37) Vishnyakov, A.; Neimark, A. V. *J. Phys. Chem. B* **2001**, *105*, 9586.
(38) Tovbin, Y. K.; Vasyatkin, N. F. *Colloids Surf. A: Physicochem. Eng. Asp.* **1999**, *158*, 385.
(39) Gebel, G. *Polymer* **2000**, *41*, 5829.
(40) Grady, B. P.; Matsuaka, H.; Nakatani, Y.; Cooper, S. L.; Ise, N. *Macromolecules* **1993**, *26*, 4064.
(41) Gebel, G.; Lambard, J. *Macromolecules* **1997**, *30*, 7914.
(42) Register, R. A.; Cooper, S. L. *Macromolecules* **1990**, *23*, 318.
(43) Chu, B.; Wang, J.; Li, Y.; Peiffer, D. G. *Macromolecules* **1992**, *25*, 4229.
(44) Ding, Y. S.; Hubard, S. L.; Hodgson, K. O.; Register, R. A.; Cooper, S. L. *Macromolecules* **1988**, *21*, 1698.
(45) Li, Y.; Peiffer, D. G.; Chu, B. *Macromolecules* **1993**, *26*, 4006.
(46) Elliot, J. A.; Hanna, S.; Elliot, A. M. S.; Cooley, G. E. *Macromolecules* **2000**, *33*, 4161.
(47) Barbi, V.; Funari, S.; Gehrke, R.; Scharnagl, N.; Stribeck, N. *Polymer* **2003**, *44*, 4853.
(48) Aldebert, P.; Dreyfus, B.; Pineri, M. *Macromolecules* **1986**, *19*, 2651.
(49) Cirkel, P. A.; Okada, T. *Macromolecules* **2000**, *33*, 4921.
(50) Cirkel, P. A.; Okada, T.; Kinugasa, S. *Macromolecules* **1999**, *32*, 531.
(51) Szajdzinska-Pietek, E.; Wolszczak, M.; Plonka, A.; Schlick, S. *Macromolecules* **1999**, *32*, 7454.
(52) Jiang, S.; Xia, K. Q.; Xu, G. *Macromolecules* **2001**, *34*, 7783.
(53) Tricoli, V.; Nannetti, F. *Electrochem. Acta* **2003**, *48*, 2625.
(54) Deng, Q.; Cable, K. M.; Moore, R. B.; Mauritz, K. A. *J. Polym. Sci., Part B, Polym. Phys.* **1996**, *34*, 1917.
(55) Nunes, S. P.; Ruffmann, B.; Rikowski, E.; Vetter, S.; Richau, K. *J. Membr. Sci.* **2002**, *203*, 215.
(56) Gambursez, S.; Appleby, A. J. *J. Power Sources* **2002**, *107*, 5.
(57) Aldebert, P.; Gebel, G.; Loppinet, B.; Nakamura, N. *Polymer* **1995**, *36*, 431.

(58) Rollet, A.-L.; Gebel, G.; Simonin, J.-P.; Turq, P. *J. Polym. Sci., Part B: Polym. Phys.* **2001**, *39*, 548.
(59) Narayanan, T.; Diat, O.; Bösecke, P. *Nucl. Inst. Methods Phys. Res. A* **2001**, *467−468*, 1005.
(60) James, P. J.; Antognozzi, M.; Tamayo, J.; McMaster, T. J.; Newton, J. M.; Miles, M. J. *Langmuir* **2001**, *17*, 349.
(61) Basset, D. C.; Davitt, R. *Polymer* **1974**, *15*, 721.
(62) Starkweather, H. W. *Macromolecules* **1982**, *15*, 320.
(63) Dobrynin, A. V.; Rubinstein, M.; Obukhov, S. P. *Macromolecules* **1996**, *29*, 2974.
(64) Waigh, T. A.; Ober, R.; Williams, C. E. *Macromolecules* **2001**, *34*, 1973.
(65) Chattopadhyay, D.; Galeska, I. E.; Papadimitrakopoulos, F.; Munoz, E.; Baughman, R. H. *Proc. SPIE−Int. Soc. Opt. Eng.* **2002**, *4695*, 52.
(66) Rollet, A.-L.; Diat, O.; Gebel, G. *J. Phys. Chem. B* **2002**, *106*, 3033.
(67) Nallet, F.; Laversanne, R.; Roux, D. *J. Phys. II* **1997**, *7*, 487.
(68) Ramsay, J. D. F.; Swanton, S. W.; Bunce, J. *J. Chem. Soc., Faraday Trans.* **1990**, *86*, 3919.
(69) Pederson, J. S. *Adv. Colloid Interface Sci.* **1997**, *70*, 171.
(70) Gebel, G. Thesis of the University J. Fourier, Grenoble, France, 1991.
(71) Debye, P.; Bueche, A. M. *J. Appl. Phys.* **1949**, *20*, 518.
(72) Debye, P.; Anderson, H. R.; Brumberger, H. *J. Appl. Phys.* **1957**, *28*, 679.
(73) Chomakova-Haefke, M.; Nyffenegger, R.; Schmidt, E. *Appl. Phys. A: Mater. Sci. Process.* **1994**, *59*, 151.
(74) Lehmani, A.; Durand, S.; Turq, P. *J. Appl. Polym. Sci.* **1998**, *68*, 503.
(75) McLean, R. S.; Doyle, M.; Sauer, B. B. *Macromolecules* **2000**, *33*, 6541.
(76) Rubatat, L.; van der Heijden, P. C.; Gebel, G.; De la Rosa, A.; Diat, O. Manuscript in preparation.
(77) Rubatat, L. Thesis of the University J. Fourier, Grenoble, France, 2003.
(78) Van der Heijden, P. C.; Rubatat, L.; Gebel, G.; Diat, O. *Macromolecules* **2004**, *37*, 5327.
(79) Hill, T. A.; Caroll, D. L.; Czerw, R.; Martin, C. W.; Perahia, D. *J. Polym. Sci., Part B: Polym. Phys.* **2003**, *41*, 149.
(80) Siroma, Z.; Fujiwara, N.; Ioroi, T.; Yamazaki, S.; Yasuda, K.; Miyazaki, Y. *J. Power Sources* **2004**, *126*, 41.

MA049683J